Local-field-corrected van der Waals potentials in magnetodielectric multilayer systems

Agnes Sambale and Dirk-Gunnar Welsch
Theoretisch-Physikalisches Institut, Friedrich-Schiller-Universität Jena, Max-Wien-Platz 1, D-07743 Jena, Germany

Ho Trung Dung
Institute of Physics, Academy of Sciences and Technology, 1 Mac Dinh Chi Street, District 1, Ho Chi Minh City, Vietnam

Stefan Yoshi Buhmann
Quantum Optics and Laser Science, Blackett Laboratory, Imperial College London, Prince Consort Road, London SW7 2AZ, United Kingdom

(Received 18 December 2008; published 4 February 2009)

Within the framework of macroscopic quantum electrodynamics in linear, causal media, we study the van der Waals potentials of ground-state atoms in planar magnetodielectric host media. Our investigation extends earlier ones in two aspects: It allows for the atom to be embedded in a medium, thus covering many more realistic systems, and it takes account of the local-field correction. Two- and three-layer configurations are treated in detail both analytically and numerically. It is shown that an interplay of electric and magnetic properties in neighboring media may give rise to potential wells or walls. Local-field corrections as high as 80% are found. By calculating the full potential including the translationally invariant and variant parts, we propose a way to estimate the (finite) value of the dispersion potential at the surface between two media. Connection with earlier work intended for biological applications is established.

DOI: 10.1103/PhysRevA.79.022903 PACS number(s): 34.35.+a, 12.20.−m, 42.50.Nn, 42.50.Wk

I. INTRODUCTION

The dispersive interaction between small neutral, unpolarized particles (atoms, molecules, etc.) and an uncharged macroscopic object is a manifestation of the quantum nature of the electromagnetic field and related to the zero-point energy [1]. In the first quantum electrodynamical treatment of this van der Waals (vdW) type force [2] and in many other related works, the atom was assumed to be located in free space. In reality, the atom may be submerged in or be a part of a gas, liquid, or even solid—a situation typical in diverse fields such as colloid science [3–5], surface engineering [6], and biology [7]. As a particular example from biology, one can cite the transfer of a small particle diluted in cell plasma through a cell membrane caused by vdW forces [8]. A question that may arise when the atom is embedded in a medium is how the vdW interaction is to be corrected due to the difference between the local fields acting on the atom and the macroscopic fields averaged over a region which contains a great number of the medium constituents, thus ignoring the gaps between them. In Ref. [9], the vdW interaction between two ground-state atoms embedded in adjacent semi-infinite magnetodielectric media has been considered. Comparison of this result with that deduced from the Casimir force on a thin composite slab in front of a composite semi-infinite medium, both obeying the Clausius-Mossotti relation, suggests a hint as to how to account for the local-field correction. This confirmed shortly after in Ref. [10] on the basis of a macroscopic quantum electrodynamics theory and real-cavity model [11]. A general formula for the vdW potential in an arbitrary geometry has been derived in the form of a sum of a translationally invariant term and and a term containing the uncorrected scattering Green tensor modified by a local-field correction factor [9,10]. This general formula is applicable for metamaterials [12] and will serve as a starting point for our treatment of the local-field-corrected vdW interaction in a stratified magnetodielectric. Note that a generalization of the formalism has recently been used to study local-field-corrected interactions of an excited atom with a ground-state one across an interface between two media [13].

The interaction between a neutral atom and a material surface is customarily split into two parts: a short-range repulsive part, significant when the atomic valence electrons overlap with the surface, and a longer-range dispersive vdW part [14–20]. Theories that focus on the vdW interaction commonly neglect the first and thus are incapable of correctly predicting the behavior of the interaction potential at very short distances. They typically yield a power law of z_A^{-3} (z_A, atom-surface distance) for materials with dominant electric properties and a power law of z_A^{-1} for purely magnetic materials, which lead to divergent values for the vdW potential right on the surface [2,21,22]. Due to the importance of phenomena such as physisorption and transport of particles through interfaces and membranes, much effort has been devoted to a better treatment of the atom-surface interaction when the two are at very short distances. With respect to physisorption, this has been done via introducing a reference plane [23]; via characterizing the material surface by a more realistic response function which includes spatial dispersion [24], smooth variation of the dielectric properties at the interface, and the contribution from d electrons to the screening [25]; and via using an atomic polarizability going beyond the dipole approximation [17,25]. These studies typically produce finite values for the interaction potential at the interface [23].

In the present paper, the local-field-corrected vdW interaction of a ground-state atom embedded in a planar, dispersing, and absorbing magnetoelectric host medium is studied within the framework of macroscopic quantum electrodynamics and the real-cavity model. We propose a procedure

that would allow for obtaining an estimate of the finite vdW energy of an atom right on the interface even within our predominantly macroscopic framework treating the atom within electric-dipole approximation. The paper is organized as follows. In Sec. II the main results concerning the local-field-corrected vdW interaction of a ground-state atom and an arbitrary absorbing and dispersing macroscopic body are reviewed and then applied to planar multilayer systems. The two-layer case is considered and a procedure for an estimation of the vdW potential at the interface is given in Sec. III, while the three-layer case is discussed in Sec. IV. Connection with earlier work which focus on biological systems and concluding remarks are given in Sec. V.

II. MODEL

We set the stage by briefly recalling the results for the local-field-corrected vdW potential of a ground-state atom within an arbitrary geometry and applying them to a planar multilayer system.

A. Local-field-corrected vdW potentials in arbitrary geometries

We consider a ground-state guest atom A located at $\mathbf{r}_A$ in an absorbing and dispersing host medium of arbitrary size and shape characterized by macroscopic $\varepsilon(\mathbf{r},\omega)$ and $\mu(\mathbf{r},\omega)$. To account for the local-field correction, we employ the real-cavity model by assuming the atom to be surrounded by a small spherical free-space cavity of radius R_c. The radius of the cavity is a measure of the distance between the guest atom and the surrounding host atoms [10]. By construction, the macroscopic quantities $\varepsilon(\mathbf{r},\omega)$ and $\mu(\mathbf{r},\omega)$ do not vary appreciably on the microscopic length scale R_c. To apply the real cavity model, one should keep in mind that $\sqrt{\varepsilon(0)\mu(0)}R_c$ should be small compared to the maximum of all characteristic atomic and medium wavelengths as well as to the separation from any surface of the host medium. In particular, the application of model to metals is very problematic. Using second-order perturbation theory, the vdW potential for such an atom can be written in the form [10]

$$U(\mathbf{r}_A) = U_1(\mathbf{r}_A) + U_2(\mathbf{r}_A), \tag{1}$$

where $U_1(\mathbf{r}_A)$ is constant throughout any homogeneous region and accounts for all scattering processes within the cavity,

$$U_1(\mathbf{r}_A) = -\frac{\hbar\mu_0}{4\pi^2 c}\int_0^\infty d\xi\xi^3\alpha(i\xi)C_A(i\xi), \tag{2}$$

where

$$C_A(\omega) = \frac{h_1^{(1)}(z_0)[zh_1^{(1)}(z)]' - \varepsilon_A(\omega)h_1^{(1)}(z)[z_0h_1^{(1)}(z_0)]'}{\varepsilon_A(\omega)h_1^{(1)}(z)[z_0j_1(z_0)]' - j_1(z_0)[zh_1^{(1)}(z)]'}, \tag{3}$$

[$z_0=\omega R_c/c$, $z=n(\omega)z_0$, $n(\omega)=\sqrt{\varepsilon_A(\omega)\mu_A(\omega)}$, $\varepsilon_A(\omega)=\varepsilon(\mathbf{r}_A,\omega)$, $\mu_A(\omega)=\mu(\mathbf{r}_A,\omega)$], with $j_1(x)$ and $h_1^{(1)}(x)$, respectively, being the first spherical Bessel function and the first spherical Hankel function of the first kind,

$$j_1(x) = \frac{\sin(x)}{x^2} - \frac{\cos(x)}{x}, \tag{4}$$

$$h_1^{(1)}(x) = -\left(\frac{1}{x} + \frac{i}{x^2}\right)e^{ix}, \tag{5}$$

and $\alpha(\omega)$ denoting the isotropic polarizability of the guest atom in lowest nonvanishing order of perturbation theory [26],

$$\alpha(\omega) = \lim_{\eta\to 0+}\frac{2}{3\hbar}\sum_k \frac{\omega_{k0}|\mathbf{d}^{0k}|^2}{\omega_{k0}^2 - \omega^2 - i\eta\omega}, \tag{6}$$

with $\omega_{k0}=(E_k-E_0)/\hbar$ being the (unperturbed) atomic transition frequencies and $\mathbf{d}^{lk}\equiv\langle k|\hat{\mathbf{d}}|l\rangle$ being the atomic electric-dipole transition matrix elements.

The term $U_2(\mathbf{r}_A)$ involves all interactions associated with the particular shape and size of the magnetodielectric host medium,

$$U_2(\mathbf{r}_A) = \frac{\hbar\mu_0}{2\pi}\int_0^\infty d\xi\xi^2 D_A^2(i\xi)\alpha(i\xi)\mathrm{Tr}\mathbf{G}^{(1)}(\mathbf{r}_A,\mathbf{r}_A,i\xi), \tag{7}$$

where

$$D_A(\omega) = \frac{j_1(z_0)[z_0h_1^{(1)}(z_0)]' - [z_0j_1(z_0)]'h_1^{(1)}(z_0)}{\mu_A(\omega)\{j_1(z_0)[zh_1^{(1)}(z)]' - \varepsilon_A(\omega)[z_0j_1(z_0)]'h_1^{(1)}(z)\}}. \tag{8}$$

The Green tensor $\mathbf{G}^{(1)}(\mathbf{r},\mathbf{r}',\omega)$ of the electromagnetic field accounts for scattering at the inhomogeneities of the (unperturbed) magnetoelectric host medium, while the factor $D_A(\omega)$ comes from the local-field correction.

Within the real-cavity model, the potentials $U_1(\mathbf{r}_A)$ and $U_2(\mathbf{r}_A)$ are well approximated by their asymptotic limit of small cavity radii; i.e., we keep only the leading nonvanishing order in $\sqrt{|\varepsilon(0)\mu(0)|}\omega_{\max}R_c/c$, where $\omega_{\max}$ represents the maximum of characteristic atomic and medium frequencies (for details, see Ref. [10])

$$U_1(\mathbf{r}_A) = -\frac{\hbar}{4\pi^2\varepsilon_0}\int_0^\infty d\xi\alpha\left[3\frac{\varepsilon_A-1}{2\varepsilon_A+1}\frac{1}{R_c^3} + \frac{9\xi^2}{c^2}\frac{\varepsilon_A^2[1-5\mu_A]+3\varepsilon_A+1}{5[2\varepsilon_A+1]^2}\frac{1}{R_c}\right] \tag{9}$$

and

$$U_2(\mathbf{r}_A) = \frac{\hbar\mu_0}{2\pi}\int_0^\infty d\xi\xi^2\alpha\left(\frac{3\varepsilon_A}{2\varepsilon_A+1}\right)^2\mathrm{Tr}\mathbf{G}^{(1)}(\mathbf{r_A},\mathbf{r_A},i\xi). \tag{10}$$

Here and in the following the dependence of ε, μ, and α on the $i\xi$ is suppressed for brevity. Note that in leading order the local-field factor $[3\varepsilon_A/(2\varepsilon_A+1)]^2$ depends on dielectric properties only. The associated (conservative) vdW force is given by

$$\mathbf{F}(\mathbf{r}_A) = -\nabla U_2(\mathbf{r}_A) = -\frac{\hbar\mu_0}{2\pi}\int_0^\infty d\xi\xi^2\alpha \times \left(\frac{3\varepsilon_A}{2\varepsilon_A+1}\right)^2 \nabla \mathrm{Tr}\mathbf{G}^{(1)}(\mathbf{r}_A,\mathbf{r}_A,i\xi). \quad (11)$$

The cavity-induced part of the potential, U_1 according to Eq. (2), does not lead to a force, but to an energy shift whose influence on the overall potential will be studied in Secs. III and IV.

B. Atom in a magnetoelectric multilayer system

So far, we have not been specific about the geometry of the macroscopic body. Consider a stack of n layers labeled by l $(l=1,\ldots,n)$ of thicknesses d_l with planar parallel boundary surfaces, where $\varepsilon(\mathbf{r},\omega)=\varepsilon_l(\omega)$ and $\mu(\mathbf{r},\omega)=\mu_l(\omega)$ in layer l. The coordinate system is chosen such that the layers are perpendicular to the z axis and extend from $z=0$ to $z=d_l$ for $l\neq 1,n$ and from $z=0$ to $z=-\infty(\infty)$ for $l=1$ (n). The scattering part of the Green tensor at imaginary frequencies for $\mathbf{r}$ and $\mathbf{r}'$ in layer j is given by (see, e.g., Ref. [22])

$$\mathbf{G}^{(1)}(\mathbf{r},\mathbf{r}',i\xi) = \int d^2q e^{i\mathbf{q}\cdot(\mathbf{r}-\mathbf{r}')}\mathbf{G}^{(1)}(\mathbf{q},z,z',i\xi) \quad (12)$$

$(\mathbf{q}\perp\mathbf{e}_z)$, where

$$\mathbf{G}^{(1)}(\mathbf{q},z,z',i\xi) = \frac{\mu_j}{8\pi^2\beta_j}\sum_{\sigma=s,p}\left\{\frac{1}{D_j^\sigma}[\mathbf{e}_\sigma^+\mathbf{e}_\sigma^- r_{j-}^\sigma e^{-\beta_j(z+z')} + \mathbf{e}_\sigma^-\mathbf{e}_\sigma^+ r_{j+}^\sigma e^{-2\beta_j d_j}e^{\beta_j(z+z')}] + \frac{r_{j-}^\sigma r_{j+}^\sigma e^{-2\beta_j d_j}}{D_j^\sigma}[\mathbf{e}_\sigma^+\mathbf{e}_\sigma^+ e^{-\beta_j(z-z')} + \mathbf{e}_\sigma^-\mathbf{e}_\sigma^- e^{\beta_j(z-z')}]\right\} \quad (13)$$

$(j>0$, for $j=0$ set $d_0=0)$, with the abbreviation

$$D_j^\sigma = 1 - r_{j-}^\sigma r_{j+}^\sigma e^{-2\beta_j d_j}. \quad (14)$$

In Eq. (13), $p(s)$ denotes $p(s)$ polarizations. The reflection coefficients obey the recursion relations

$$r_{l\pm}^\sigma = \frac{r_{ll\pm1}^\sigma + e^{-2\beta_{l\pm1}d_{l\pm1}}r_{l\pm1\pm}^\sigma}{1 + r_{ll\pm1}^\sigma r_{l\pm1\pm}^\sigma e^{-2\beta_{l\pm1}d_{l\pm1}}}, \quad (15)$$

$$r_{ll+1}^p = \frac{\varepsilon_{l+1}\beta_l - \varepsilon_l\beta_{l+1}}{\mu_{l+1}\beta_l + \varepsilon_l\beta_{l+1}}, \quad r_{ll+1}^s = \frac{\mu_{l+1}\beta_l - \mu_l\beta_{l+1}}{\mu_{l+1}\beta_l + \mu_l\beta_{l+1}} \quad (16)$$

$(r_{1-}^\sigma = r_{n+}^\sigma = 0)$, where the modulus of wave vector in the z direction is given by

$$\beta_l = \sqrt{k_l^2 + q^2}, \quad (17)$$

with k_l, which always appears in the form of k_l^2 in the Green tensor, Eq. (13), being

$$k_l^2 = \frac{\xi^2}{c^2}\varepsilon_l\mu_l. \quad (18)$$

The s- and p-polarization unit vectors are defined as

$$\mathbf{e}_s^\pm = \mathbf{e}_q \times \mathbf{e}_z, \quad \mathbf{e}_p^\pm = \frac{1}{ik_j}(q\mathbf{e}_z \mp i\beta_j\mathbf{e}_q) \quad (19)$$

$(\mathbf{e}_q=\mathbf{q}/q,\ q=|\mathbf{q}|)$. Substitution of Eqs. (12) and (13) into Eq. (10) leads to

$$U_2(z_A) = \frac{\hbar\mu_0}{8\pi^2}\int_0^\infty d\xi\xi^2\alpha\mu_j\left[\frac{3\varepsilon_j}{2\varepsilon_j+1}\right]^2 \times \int_0^\infty dq\frac{q}{\beta_j}\left\{e^{-2\beta_j z_A}\left[\frac{r_{j-}^s}{D_j^s} - \left(1+2\frac{q^2c^2}{\xi^2\varepsilon_j\mu_j}\right)\frac{r_{j-}^p}{D_j^p}\right] + e^{-2\beta_j(d_j-z_A)}\left[\frac{r_{j+}^s}{D_j^s} - \left(1+2\frac{q^2c^2}{\xi^2\varepsilon_j\mu_j}\right)\frac{r_{j+}^p}{D_j^p}\right]\right\} + \frac{\hbar\mu_0}{4\pi^2}\int_0^\infty d\xi\,\xi^2\alpha\mu_j\left[\frac{3\varepsilon_j}{2\varepsilon_j+1}\right]^2 \times \int_0^\infty dq\frac{q}{\beta_j}\sum_{\sigma=s,p}\frac{r_{j-}^\sigma r_{j+}^\sigma e^{-2\beta_j d_j}}{D_j^\sigma}, \quad (20)$$

where we have used the relations

$$\mathbf{e}_s^\pm\cdot\mathbf{e}_s^\pm = \mathbf{e}_s^\pm\cdot\mathbf{e}_s^\mp = 1, \quad (21)$$

$$\mathbf{e}_p^\pm\cdot\mathbf{e}_p^\pm = 1, \quad \mathbf{e}_p^\pm\cdot\mathbf{e}_p^\mp = -1 - 2\frac{q^2c^2}{\xi^2\varepsilon_j\mu_j} \quad (22)$$

to calculate the trace. It is worth noting that the term in curly brackets in Eq. (20) describes processes that involve an odd number of reflections at the interfaces, while the second term accounts for an even number of reflections, as can be seen from

$$\frac{r_{j-}^\sigma e^{-2\beta_j z_A}}{1 - r_{j-}^\sigma r_{j+}^\sigma e^{-2\beta_j d_j}} = e^{-\beta_j z_A}r_{j-}^\sigma e^{-\beta_j z_A} + e^{-\beta_j z_A}r_{j-}^\sigma e^{-\beta_j d_j}r_{j+}^\sigma e^{-\beta_j d_j}r_{j-}^\sigma e^{-\beta_j z_A} + \cdots, \quad (23)$$

$$\frac{r_{j+}^\sigma e^{-2\beta_j(d_j-z_A)}}{1 - r_{j-}^\sigma r_{j+}^\sigma e^{-2\beta_j d_j}} = e^{-\beta_j(d_j-z_A)}r_{j+}^\sigma e^{-\beta_j(d_j-z_A)} + e^{-\beta_j(d_j-z_A)}r_{j+}^\sigma e^{-\beta_j d_j}r_{j-}^\sigma e^{-\beta_j(d_j-z_A)} + \cdots, \quad (24)$$

and

$$\frac{r_{j-}^\sigma r_{j+}^\sigma e^{-2\beta_j d_j}}{1 - r_{j-}^\sigma r_{j+}^\sigma e^{-2\beta_j d_j}} = e^{-\beta_j z_A}r_{j-}^\sigma e^{-\beta_j d_j}r_{j+}^\sigma e^{-\beta_j(d_j-z_A)} + e^{-\beta_j z_A}r_{j-}^\sigma e^{-\beta_j d_j}r_{j+}^\sigma e^{-\beta_j d_j} \times r_{j-}^\sigma e^{-\beta_j d_j}r_{j+}^\sigma e^{-\beta_j(d_j-z_A)} + \cdots. \quad (25)$$

Obviously, the expression presented in Eq. (25), which corresponds to even numbers of reflections, is independent of the position of the atom and rapidly decreases with increasing distance between two plates. Hence, it cannot lead to a force, but only to a layer-dependent energy shift which is small compared to the other terms. It is completely absent in the two-layer case since only single reflections at the inter-

face occur. It also vanishes for sufficiently dilute media, an expansion for small $\chi_j=\varepsilon_j-1$ and $\zeta_j=\mu_j-1$ showing no contribution to linear order, which reflects the fact that at least three medium-assisted reflection processes are involved. On the contrary, Eqs. (23) and (24) depend on the position of the atom, where waves propagating to the left and right of the atom have to be distinguished.

It is worth noting that all formulas in this section are valid for arbitrary (passive) magnetoelectric media, including metamaterials and, in particular, left-handed materials with simultaneously negative real parts of ε and μ, due to the fact that $\sqrt{\varepsilon_j(\omega)\mu_j(\omega)}$ has no branching points in the upper half of the complex frequency plane. However, left-handed material properties being only realized in finite-frequency windows, they cannot be expected to have a strong influence on ground-state dispersion potentials, which depend on the medium response at all frequencies; alternatively, this can be seen from the fact that the potential is expressible in terms of permittivities and permeabilities taken at imaginary frequencies which are always positive [22,27]. The situation can change when the atom is in an excited state and the atom-field interaction resonantly depends on the medium response at the atomic transition frequencies [28,29].

III. vdW POTENTIAL NEAR AN INTERFACE

Let us first apply the theory to the simplest case of a single interface between two homogeneous semi-infinite magnetoelectric half-spaces, where we first concentrate on the position-dependent part of the potential responsible for the vdW force and then interpret the (layer-dependent) constant part.

A. Position-dependent part

For a planar magnetoelectric two-layer system with the guest atom placed in, say, layer 2, substitution of $r^{\sigma}_{n+}=0$ and r^{σ}_{n-} in accordance with Eqs. (16) in Eq. (20) leads to the following expression for the position-dependent part of the vdW potential:

$$U_2(z_A)=\frac{\hbar\mu_0}{8\pi^2}\int_0^\infty d\xi\xi^2\alpha\left(\frac{3\varepsilon_2}{2\varepsilon_2+1}\right)^2 \times\mu_2\int_0^\infty dq\frac{q}{\beta_2}\left[\frac{\mu_1\beta_2-\mu_2\beta_1}{\mu_1\beta_2+\mu_2\beta_1} -\frac{\varepsilon_1\beta_2-\varepsilon_2\beta_1}{\varepsilon_1\beta_2+\varepsilon_2\beta_1}\left(1+2\frac{q^2c^2}{\varepsilon_2\mu_2\xi^2}\right)\right]e^{-2\beta_2 z_A}, \quad (26)$$

which differs from its atom-in-free-space counterpart by the local-field correction factor $[(3\varepsilon_2)/(2\varepsilon_2+1)]^2$ and by $\varepsilon_2\neq 1$ and $\mu_2\neq 1$ [22].

1. Retarded limit

It is instructive to study the potential in the retarded limit

$$z_A\gg\frac{c}{\omega_A^-}\quad\text{and}\quad z_A\gg\frac{c}{\omega_M^-}, \quad (27)$$

with ω_A^- and ω_M^- being the minima of all relevant atomic transition and medium resonance frequencies, respectively. Introducing an integration variable $v=c\beta_2/\xi$ and replacing $\alpha(i\xi)\simeq\alpha(0)$, $\varepsilon_{1,2}(i\xi)\simeq\varepsilon_{1,2}(0)$, and $\mu_{1,2}(i\xi)\simeq\mu_{1,2}(0)$, the integration over ξ can be performed and we obtain for the potential

$$U_2(z_A)=\frac{C_4}{z_A^4}, \quad (28)$$

where

$$C_4=\frac{3\hbar c}{64\varepsilon_0\pi^2}\alpha(0)\left(\frac{3\varepsilon_2(0)}{2\varepsilon_2(0)+1}\right)^2\mu_2(0)\int_{\sqrt{\varepsilon_2(0)\mu_2(0)}}^\infty dv \times\frac{1}{v^4}\left[\frac{\mu_1(0)v-\mu_2(0)\sqrt{v^2-\varepsilon_2(0)\mu_2(0)+\varepsilon_1(0)\mu_1(0)}}{\mu_1(0)v+\mu_2(0)\sqrt{v^2-\varepsilon_2(0)\mu_2(0)+\varepsilon_1(0)\mu_1(0)}} +\frac{\varepsilon_1(0)v-\varepsilon_2(0)\sqrt{v^2-\varepsilon_2(0)\mu_2(0)+\varepsilon_1(0)\mu_1(0)}}{\varepsilon_1(0)v+\varepsilon_2(0)\sqrt{v^2-\varepsilon_2(0)\mu_2(0)+\varepsilon_1(0)\mu_1(0)}} \times\left(1-2\frac{v^2}{\varepsilon_2(0)\mu_2(0)}\right)\right]. \quad (29)$$

It can be proven that $\partial C_4/\partial\varepsilon_1(0)<0$, $\partial C_4/\partial\mu_1(0)>0$, and $\partial C_4/\partial\mu_2(0)<0$.

To deduce some physics from Eq. (29), we consider some limiting cases. Assuming that the atom is located in free space, $\mu_2(0)=\varepsilon_2(0)=1$, it can be shown that, for a purely electric half-space 1,

$$C_4[\mu_1(0)=1,\mu_2(0)=1,\varepsilon_2(0)=1]<0 \quad (30)$$

and, for a purely magnetic half-space 1 with $\mu_1(0)>1$,

$$C_4[\varepsilon_1(0)=1,\mu_2(0)=1,\varepsilon_2(0)=1]>0. \quad (31)$$

The inequality (30) means the atom is attracted toward the electric half-space—the case that is commonly treated in earlier literature. On the other hand, the positivity of C_4 in Eq. (31) means the atom is repelled from the magnetic half-space. This, coupled with the signs of the derivatives given below Eq. (29), implies that electric properties tend to make the potential attractive, while magnetic ones tend to make the potential repulsive.

Now, if the atom is embedded in a material half-space, while the opposite half-space is empty, $\mu_1(0)=\varepsilon_1(0)=1$, it can be shown that, for a purely electric material,

$$C_4[\mu_1(0)=1,\varepsilon_1(0)=1,\mu_2(0)=1]>0, \quad (32)$$

the atom is repulsed from the interface, while for a purely magnetic material with $\mu_2(0)>1$,

$$C_4[\mu_1(0)=1,\varepsilon_1(0)=1,\varepsilon_2(0)=1]<0, \quad (33)$$

the atom is attracted towards the interface. Since $\partial C_4/\partial\mu_2(0)<0$, if one starts from a purely electric material which is accompanied by a repulsive potential and then enhances the magnetic properties of the material by increasing $\mu_2(0)$, one would obtain with an attractive potential in accordance with Eq. (33).

Another particular case is when the magnetodielectric contrast between the contacting media is small,

$$\varepsilon_1(0)=\varepsilon_2(0)+\chi(0), \quad (34)$$

$$\mu_1(0) = \mu_2(0) + \zeta(0). \tag{35}$$

$[\chi(0) \ll \varepsilon_2(0),\ \zeta(0) \ll \mu_2(0)]$, one can further treat the integrals analytically by keeping only terms linear in χ and ζ:

$$\frac{\mu_1(0)v - \mu_2(0)\sqrt{v^2 - \varepsilon_2(0)\mu_2(0) + \varepsilon_1(0)\mu_1(0)}}{\mu_1(0)v + \mu_2(0)\sqrt{v^2 - \varepsilon_2(0)\mu_2(0) + \varepsilon_1(0)\mu_1(0)}} \simeq \left(\frac{1}{2\mu_2(0)} - \frac{\varepsilon_2(0)}{4v^2}\right)\zeta(0) - \frac{\mu_2(0)}{4v^2}\chi(0), \tag{36}$$

$$\frac{\varepsilon_1(0)v - \varepsilon_2(0)\sqrt{v^2 - \varepsilon_2(0)\mu_2(0) + \varepsilon_1(0)\mu_1(0)}}{\varepsilon_1(0)v + \varepsilon_2(0)\sqrt{v^2 - \varepsilon_2(0)\mu_2(0) + \varepsilon_1(0)\mu_1(0)}} \simeq -\frac{\varepsilon_2(0)}{4v^2}\zeta(0) + \left(\frac{1}{2\varepsilon_2(0)} - \frac{\mu_2(0)}{4v^2}\right)\chi(0). \tag{37}$$

The v integration is straightforward, and we arrive at

$$C_4 = \frac{9\hbar c}{640\pi^2\varepsilon_0}\alpha(0)\frac{-23\mu_2(0)\chi(0) + 7\varepsilon_2(0)\zeta(0)}{\sqrt{\varepsilon_2(0)\mu_2(0)}\mu_2(0)[2\varepsilon_2(0)+1]^2}. \tag{38}$$

This result generalizes the one obtained in Ref. [22] to the case of an atom embedded in a medium, with local-field correction included. It is richer in content than its atom-in-free-space counterpart. For example, when $\chi(0)=\zeta(0)$ and the atom in free space $\varepsilon_2(0)=\mu_2(0)=1$, the potential is attractive, whereas when the atom is in a medium of $\varepsilon_2(0)/\mu_2(0) > 23/7$, a repulsive potential can be realized.

2. Nonretarded limit

The nonretarded limit corresponds to atom-surface distances z_A small compared with the typical wavelengths of the medium and the atomic system:

$$z_A \ll \frac{c}{\omega_A^+[n_1(0)+n_2(0)]} \tag{39}$$

and/or

$$z_A \ll \frac{c}{\omega_M^+[n_1(0)+n_2(0)]} \tag{40}$$

$[n_{1,2}(0)=\sqrt{\varepsilon_{1,2}(0)\mu_{1,2}(0)}$; ω_A^+ and ω_M^+, maxima of the relevant atomic transition and medium resonance frequencies]. The conditions (39) and (40) imply

$$\frac{\xi z_A}{c}\sqrt{|\varepsilon_1\mu_1 - \varepsilon_2\mu_2|} \ll 1, \tag{41}$$

$$\frac{\xi z_A}{c}\sqrt{\varepsilon_2\mu_2} \ll 1, \tag{42}$$

where we have used the fact that the ξ integration is practically limited to a region where $\xi \lesssim \omega_{A,M}^+$. We substitute

$$q = \sqrt{\beta_2^2 - \varepsilon_2\mu_2\xi^2/c^2}, \tag{43}$$

$$q\,dq = \beta_2 d\beta_2, \tag{44}$$

$$\beta_1 = \sqrt{\xi^2/c^2(\varepsilon_1\mu_1 - \varepsilon_2\mu_2) + \beta_2^2} \tag{45}$$

in Eq. (26) and, on recalling Eq. (41), perform a leading-order Taylor expansion in $\xi^2/(c^2\beta_2^2)(\varepsilon_1\mu_1 - \varepsilon_2\mu_2)$. After carrying out the β_2 integration, we arrive at

$$U_2(z_A) = -\frac{C_3}{z_A^3} + \frac{C_1}{z_A}, \tag{46}$$

where

$$C_3 = \frac{\hbar}{16\pi^2\varepsilon_0}\int_0^\infty d\xi\,\alpha\frac{9\varepsilon_2}{(2\varepsilon_2+1)^2}\frac{\varepsilon_1-\varepsilon_2}{\varepsilon_1+\varepsilon_2}, \tag{47}$$

$$C_1 = \frac{\hbar\mu_0}{16\pi^2}\int_0^\infty d\xi\,\xi^2\alpha\mu_2\left(\frac{3\varepsilon_2}{2\varepsilon_2+1}\right)^2\left[\frac{\mu_1-\mu_2}{\mu_1+\mu_2} + \frac{\varepsilon_1-\varepsilon_2}{\varepsilon_1+\varepsilon_2} + \frac{2\varepsilon_1(\varepsilon_1\mu_1-\varepsilon_2\mu_2)}{\mu_2(\varepsilon_1+\varepsilon_2)^2}\right], \tag{48}$$

and Eq. (42) has been used to set $\exp(-2\sqrt{\varepsilon_2\mu_2}\xi z_A/c)$ equal to 1. By putting $\varepsilon_2=\mu_2=1$, Eqs. (47) and (48) reduce to those for an atom in free space [22].

As can be seen from Eqs. (46) and (47), one can distinguish two regimes having different power laws. The first regime is where the two contacting media have unequal electric properties. Then the first term in Eq. (46) dominates, and the power law is z_A^{-3}. The atom is pulled toward (repelled from) the interface if the medium it is located in has stronger (weaker) electric properties than that on the other side of the interface.

In the case of equal electric properties $C_3=0$ and $U_2(z_A)=C_1/z_A$, with

$$C_1 = \frac{\hbar\mu_0}{16\pi^2}\int_0^\infty d\xi\,\xi^2\alpha\left(\frac{3\varepsilon_2}{2\varepsilon_2+1}\right)^2(\mu_1-\mu_2)\left(\frac{\mu_2}{\mu_1+\mu_2}+\frac{1}{2}\right). \tag{49}$$

The atom experiences a force which points away from (toward) the interface if the magnetic properties of the medium the atom is situated in are weaker (stronger) than those of the medium on the other side of the interface.

Note that the dependence of the directions of the forces on the difference in strength of the medium responses is opposite in the two cases of dominantly electric and purely magnetic media. In both cases the strength of the force increases with increasing difference between the electric and magnetic parameters of the contacting media. These results are consistent with earlier ones [8,30]. A more detailed comparison of our results with those presented in Ref. [8] will be made in the last section. Since the coefficient C_3 of the leading-order term depends on electric properties only, the influence of electric properties on the behavior of the potential tends to dominate that of the magnetic properties, except for the case when the electric properties of the neighboring media are similar. At more moderate distances, competing effects of electric and magnetic properties may create potential walls or wells, as is also evident from the numerical results below.

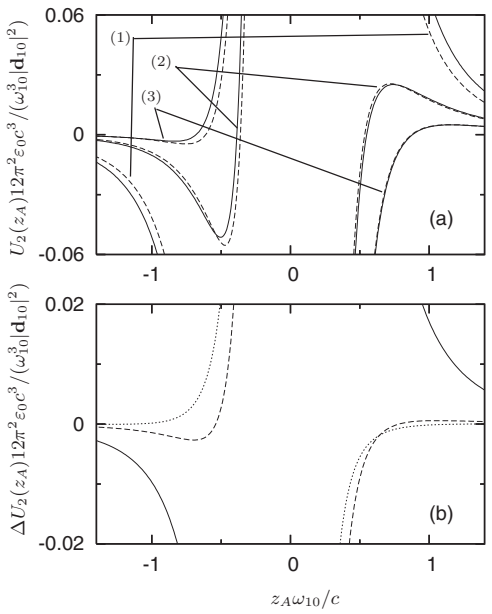

FIG. 1. (a) Position-dependent part of the vdW potential experienced by a ground-state two-level atom in a magnetoelectric two-layer system as a function of atom-surface distance for fixed ε_1, μ_1, and μ_2 and for $\omega_{Pe2}/\omega_{10}=1$ (1), 0.4 (2), and 0.2 (3). Solid lines denote the potentials with the local-field correction, while dashed lines represent those without. Other parameters are $\omega_{Te1}/\omega_{10}=\omega_{Te2}/\omega_{10}=1.03$, $\omega_{Pe1}/\omega_{10}=0.75$, $\omega_{Tm1}/\omega_{10}=\omega_{Tm2}/\omega_{10}=1$, $\omega_{Pm1}/\omega_{10}=2.3$, $\omega_{Pm2}/\omega_{10}=0.4$, and $\gamma_{m1,2}/\omega_{10}=\gamma_{e1,2}/\omega_{10}=0.001$, and the cavity radius is $R_c\omega_{10}/c=0.01$. (b) Difference between local-field-corrected and uncorrected (position-dependent) vdW potential ΔU_2 versus atom-surface distance where the solid, dashed, and dotted lines refer to the curves (1), (2), and (3), respectively.

3. Numerical results

To study the local-field-corrected potential at intermediate distances and to elucidate the combined influence of electric and magnetic properties of the media, we calculate the position-dependent part $U_2(z_A)$ in accordance with Eq. (26) numerically. A two-level atom of transition frequency ω_{10} is assumed, and material electric and magnetic properties are described using single-resonance Drude-Lorentz-type permittivities and permeabilities

$$\varepsilon_i(\omega) = 1 + \frac{\omega_{Pei}^2}{\omega_{Tei}^2 - \omega^2 - i\omega\gamma_{ei}}, \tag{50}$$

$$\mu_i(\omega) = 1 + \frac{\omega_{Pmi}^2}{\omega_{Tmi}^2 - \omega^2 - i\omega\gamma_{mi}}, \quad i = 1,2. \tag{51}$$

Figure 1(a) illustrates the atom-surface-distance dependence of the $U_2(z_A)$ potential. The interface is at $z_A=0$, and medium 1 is on the left, while medium 2 is on the right. The parameters ε_1, μ_1, and μ_2 are fixed, whereas ε_2 takes on three different values of the plasma frequency ω_{Pe2}. In all three cases ε_1 and ε_2 have the same (transverse) resonance frequencies ω_{Te} and damping constants γ_e, but different plasma frequencies (i.e., $\varepsilon_1 \neq \varepsilon_2$), and the z_A^{-1} term in Eq. (46) is negligibly small. In case (1), $\varepsilon_2 > \varepsilon_1$, it can be seen from the figure that the potential at very short atom-surface distances is repulsive in medium 2 and attractive in medium 1, consistent with the analytical result (46) and (47). Similarly, in cases (2) and (3), $\varepsilon_2 < \varepsilon_1$, the potential is attractive in medium 2 while repulsive in medium 1. As the atom-surface distance increases, the second term $\frac{C_1}{z_A}$ in the potential (46) gradually comes into play and, if the magnetic properties are strong enough, may switch the sign of the potential and create potential walls or wells in the process, as is clearly visible in case (2).

To show how the net effect of the local-field correction depends on the distance and on the properties of the media surrounding the guest atom, we plot the uncorrected potential by dashed lines in Fig. 1(a) and the difference between the corrected and uncorrected results in Fig. 1(b). The ratio between the corrected and uncorrected results is not always a good measure of the difference between the two because one of them can vanish. The local-field correction factor $[3\varepsilon_j/(2\varepsilon_j+1)]^2$ is positive, larger than 1, and increases with ε_j (j indicative of the layer containing the guest atom). It approaches the maximum value of 9/4 as $\varepsilon_j \to \infty$. Note that a larger-than-unity local-field correction factor does not necessarily lead to an enhancement of the potential because the uncorrected factor in the integrand can change sign as ξ varies. The local-field correction has a clear-cut effect of increasing or decreasing the potential only when the uncorrected integrand is purely repulsive or attractive, for which cases (1) and (3) can serve as examples. In the middle case (2), the two curves with and without local-field correction cross; that is, there exists an atom-surface distance at which the effect of the local-field correction is canceled out due to the ξ integration. In addition, one can notice that the local-field correction leads a small shift of the position of the peak. Figure 1(b), which shows the difference between the local-field-corrected and uncorrected potentials, reveals quite significant corrections of up to 30% of the uncorrected values.

The behavior of the local-field-corrected vdW potential with respect to the static permittivity of the medium the atom is embedded in is shown in Fig. 2 for two different values of the atom-surface distance. Within the scale of the figure, the curves for the larger distance from the interface peak at certain values of $\varepsilon_2(0)$. The positions of the peaks are different due to the effects of the local field. As ω_{Pe2}/ω_{10} and as a consequence $\varepsilon_2(0)$ increase, an inspection of the figure reveals that the ratio between the corrected and uncorrected curves tends to the static value of the local-field correction factor $\{3\varepsilon_2(0)/[2\varepsilon_2(0)+1]\}^2$ (which lies between 1 and 9/4), in agreement with the analytical analysis given in Sec. III A 1. For the smaller value of the atom-surface distance $z_A\omega_{10}/c=0.01$, a crossing point between the corrected and uncorrected curves is observed, where the local-field correction produces no net change.

B. Layer-dependent constant part

Figure 3 shows the dependence of the constant part U_1 of the potential on the real-cavity radius R_c. To gain some insight, we consider the two limiting cases of a purely electric

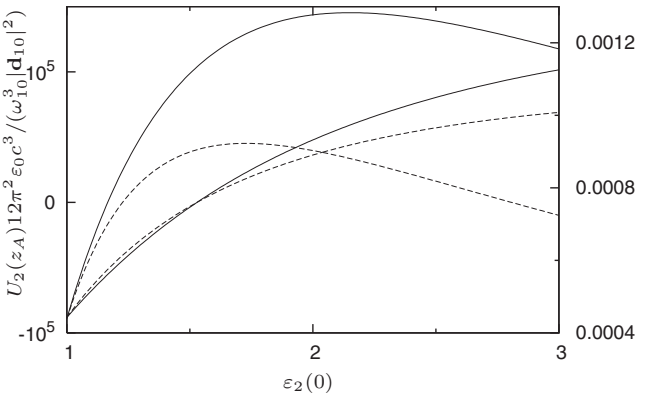

FIG. 2. Position-dependent part of the vdW potential as a function of the static permittivity $\varepsilon_2(0)$ (more specifically ω_{Pe2}/ω_{10}) for two values of the atom-surface distance $z_A\omega_{10}/c=0.01$ (scale to the left) and $z_A\omega_{10}/c=3$ (scale to the right). Solid lines are with the local-field correction, while dashed lines are without one. Other parameters are the same as in Fig. 1. Note the arrows, which indicate the ordinate scale to be used.

and a purely magnetic material. According to the analytic result (9), in the first case the leading term is proportional to $[R_c\omega_{10}/c]^{-3}$, while in the second case the leading term is proportional to $[R_c\omega_{10}/c]^{-1}$. Thus, for small enough $R_c\omega_{10}/c$, $|U_1|$ for a pure electric material is generally larger than that for a pure magnetic material—a fact that is confirmed by the figure. It can be seen that $U_1<0$ in the first case and $U_1>0$ in the second case, again in agreement with Eq. (9). The figure also indicates that the magnitude of U_1, which is entirely due to the local-field correction, decreases with an increasing real-cavity radius; that is, the effects of the local field become weaker as the medium becomes more dilute.

For comparison, we also plot the potential U_1 according to the approximate result (9) (dashed curves). It can be seen

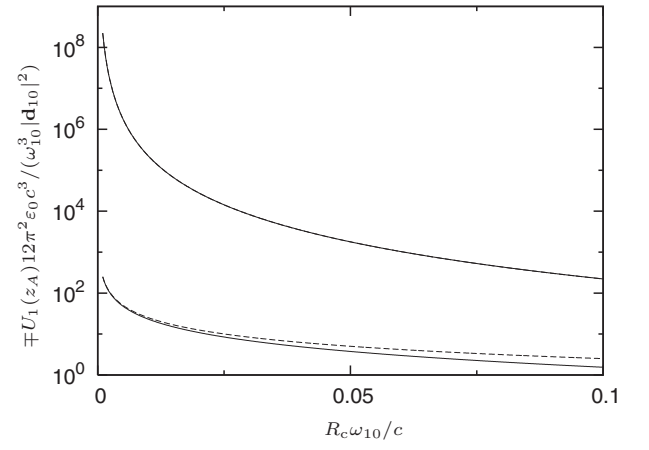

FIG. 3. The exact layer-dependent constant part of the potential (solid line), Eq. (2), and approximate results (dashed line), Eq. (9), are shown as functions of the real-cavity radius. The upper pair of curves shows $-U_1(z_A)12\pi^2\varepsilon_0 c^3/(\omega_{10}^3|\mathbf{d}_{10}|^2)$ (the sign has been reversed so that a logarithmic scale can be used) for a pure electric material with $\omega_{Pe2}/\omega_{10}=0.4$, while the lower pair of curves shows $U_1(z_A)12\pi^2\varepsilon_0 c^3/(\omega_{10}^3|\mathbf{d}_{10}|^2)$ for a pure magnetic material with $\omega_{Pm2}/\omega_{10}=0.4$. All other parameters are the same as in Fig. 1. The radius of the cavity $R_c\omega_{10}/c$ starts from 0.001.

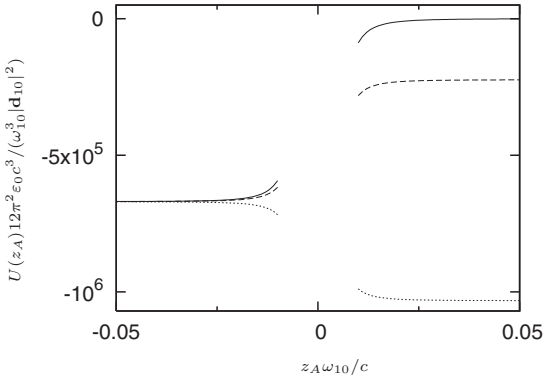

FIG. 4. Local-field-corrected total vdW potential of a ground-state two-level atom in a magnetodielectric two-layer system as a function of the atom-surface distance. Different curves are for different (equal) electric and magnetic coupling strengths of medium 2: $\omega_{Pm2}/\omega_{10}=\omega_{Pe2}/\omega_{10}=0$ (solid line), 0.4 (dashed line), and 1 (dotted line). Other parameters are the same as in Fig. 1.

that for the parameters used in the figure, the approximate result reproduces quite well the exact one, especially in the case of a pure electric material. The agreement in the case of a pure magnetic material is good for very small $R_c\omega_{10}/c$, but worsens as $R_c\omega_{10}/c$ increases.

C. Total vdW potential and its value at the interface

We have separately investigated the position-dependent part $U_2(z_A)$ of the potential, which determines the force acting on the atom, and the constant, layer-dependent part U_1, which is related to the local-field correction. For problems such as the transfer of an atom or a small particle through an interface, it is of relevance to evaluate the potential right at the interface. For this purpose, the total value of the potential is needed. In Fig. 4, we have calculated $U_1+U_2(z_A)$ on both sides of the interface with medium 1 fixed with medium 2 varying from vacuum to a more dense medium with balanced electric and magnetic properties. The case represented by the dashed line is nothing else rather than case (2) in Fig. 1. Only very short distances $\sqrt{|\varepsilon_i\mu_i|}z_A\omega_{10}/c\ll 1$ are presented. Since $\varepsilon_1\neq\varepsilon_2$ in general, the position dependence of the potential at short distances is mostly determined by the $\frac{C_3}{z_A^3}$ term, which contains $\varepsilon_1-\varepsilon_2$ in the integrand. Numerical results in the figure are consistent with this and show that the potential is attractive (repulsive) if the atom is located in a medium that is electrically more dilute (dense) than that in the opposite side of the interface. Additional structures in U_2 such as potential wells or walls are typically overwhelmed by the magnitude of U_1. Baring the visual suppression of the potential wells or walls in U_2 due to the large magnitude of U_1, a full potential is more straightforward than U_2 alone in predicting the movement of an atom across a surface. Take, for example, case (2) in Fig. 1. An atom located in layer 2 close to the surface will be attracted to it, and if the atom can cross the interface, it will be pushed further away from the surface into layer 1. Figure 4 (dashed line) provides us with some additional information. It shows explicitly that the total potential in layer 2 is higher that that in layer 1 by giving the

difference between the potentials in the two layers, and it may also help to estimate the amount of energy required for the atom to penetrate into layer 1.

In Fig. 4, we have not displayed the results for distances $|z_A| < R_c\sqrt{|\varepsilon\mu|}$ where the real-cavity model can no longer be applied. This gives rise to a gap between the potentials on the two sides of the interface. To extend our theory so that it can be employed to estimate the potential right at the interface, we suggest that

$$U(z_A=0) = \frac{1}{2}[U(R_c) + U(-R_c)]$$
$$= -\frac{\hbar}{32\pi^2\varepsilon_0 R_c^3}\int_0^\infty d\xi\,\alpha\left\{12\left(\frac{\varepsilon_1-1}{2\varepsilon_1+1}+\frac{\varepsilon_2-1}{2\varepsilon_2+1}\right)\right.$$
$$\left.-\frac{\varepsilon_1-\varepsilon_2}{\varepsilon_1+\varepsilon_2}\left[\frac{1}{\varepsilon_1}\left(\frac{3\varepsilon_1}{2\varepsilon_1+1}\right)^2-\frac{1}{\varepsilon_2}\left(\frac{3\varepsilon_2}{2\varepsilon_2+1}\right)^2\right]\right\} \tag{52}$$

[recall Eqs. (9), (46), and (47)]. Visually, this means first plotting the potential as a function of the atomic position up to distances $|z_A|=R_c$ (R_c being the radius of the cavity in the real-cavity model) and then connecting the two loose ends on the two sides of the interface to find the value of the potential at $z_A=0$. Our result is remarkably similar to what has been obtained by calculating the on-surface potential of a molecule of finite size s [31]:

$$U(z_A=0) = \frac{\hbar}{2\pi^{5/2}\varepsilon_0 s^3}\int_0^\infty d\xi\,\alpha\left[\frac{1}{2}\left(\frac{1}{\varepsilon_1}+\frac{1}{\varepsilon_2}\right)\right.$$
$$\left.+\frac{1}{3}\frac{\varepsilon_1-\varepsilon_2}{\varepsilon_1+\varepsilon_2}\left(\frac{1}{\varepsilon_1}-\frac{1}{\varepsilon_2}\right)\right]. \tag{53}$$

The second terms in Eqs. (52) and (53), which represent the interface contribution to the potential, agree when setting $s=(\sqrt[3]{16/3}/\pi^{-1/6})R_c \approx 1.4R_c$ and neglecting the local-field correction in Eq. (52), which was not considered in Ref. [31]. The first terms, which represent bulk contributions from the two interfacing media, differ in the two approaches, where Eq. (53) still contains self-energy contributions which do not vanish in the vacuum case $\varepsilon_i=1$, while Eq. (52) does not. Our result (52) thus represents an improvement of the previous one (53) in that local-field corrections are taken into account and self-energy contributions have consistently been removed.

IV. THREE-LAYER SYSTEM

A system consisting of an atom in a three-layer planar structure can serve as a prototype for the problem of a small particle near or inside a membrane [8]. The translationally invariant part and position-dependent part of the vdW potential can again be determined in accordance with Eqs. (2) and (20), respectively. If the atom is in one of the two outer layers, Eq. (20) simplifies greatly via either $r_{j+}^{\sigma}=0$ or $r_{j-}^{\sigma}=0$. If the atom is in the middle layer, the overall form of the potential $U_2(z_A)$ remains as in Eq. (20) and there exists a term which contains the product $r_{j-}^{\sigma}r_{j+}^{\sigma}$ and is position independent. This position-independent term in $U_2(z_A)$ is irrelevant when it is the force that is concerned, but has to be kept, together with U_1, if the potential at the surfaces is of interest. Since the formulas are complicated, we resort to numerical computation.

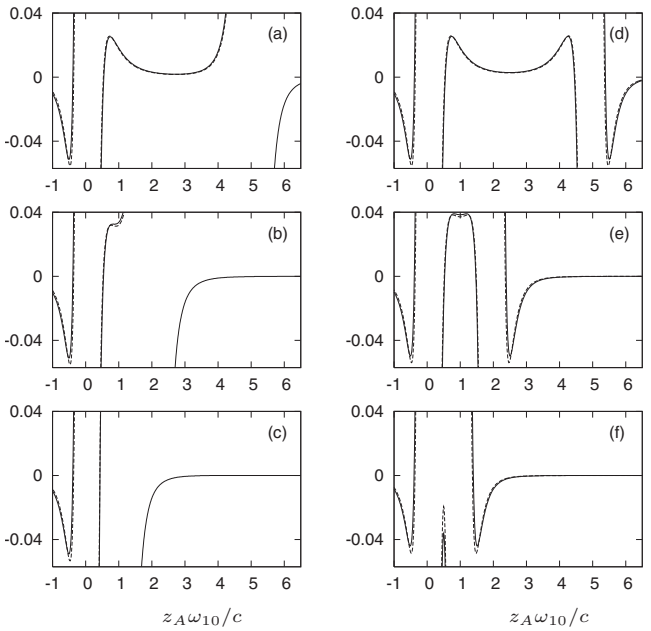

FIG. 5. Position-dependent part of the vdW potential as a function of $z_A\omega_{10}/c$ for three different thicknesses of the middle layer $d_2\omega_{10}/c=5$ [(a) and (d)], 2 [(b) and (e)], and 1 [(c) and (f)]. For the left column, the configuration is asymmetric with $\omega_{Te1}/\omega_{10}=1.03$, $\omega_{Pe1}/\omega_{10}=0.75$, $\omega_{Tm1}/\omega_{10}=1$, $\omega_{Pm1}/\omega_{10}=2.3$, $\omega_{Tm2}/\omega_{10}=1$, $\omega_{Pm2}/\omega_{10}=0.4$, $\omega_{Te2}/\omega_{10}=1.03$, $\omega_{Pe2}/\omega_{10}=0.4$, $\gamma_{m2,1}=\gamma_{e2,1}=0.001\omega_{10}$, $\varepsilon_3=\mu_3=1$, and $R_c\omega_{10}/c=0.01$. For the right column, the configuration is symmetric with the vacuum in layer 3 being replaced by a medium of the same characteristics as those of layer 1. The curves without the local-field correction are shown by dashed lines.

Figure 5 shows the behavior of the vdW potential for an atom placed in an asymmetric (left column) and a symmetric (right column) three-layer magnetodielectric structure for different thicknesses of the middle layer. Note that the parameters for layer 1 are the same as those for layer 1 in Fig. 1 and the parameters for layer 2 are the same as those for layer 2, case (2), in Fig. 1. That is, the interface 1-2 here is the same as the interface 1-2 in Fig. 1, case (2). In the asymmetric configuration, layer 3 is vacuum, while in the symmetric configuration, layers 3 and 1 have the same characteristics.

Let us first analyze the asymmetric configuration and see how the presence of a third layer 3 on the right, which is the vacuum, affects the behavior of the potential near the 1-2 interface. In case (a) where the middle-layer thickness $d_2\omega_{10}/c=5$ is the largest among the three cases, the behavior of the potential $U_2(z_A)$ in the boundary regions is similar to that in the two-layer systems. Near the 1-2 interface, we find a potential well in layer 1 and a potential wall in layer 2, just as in Fig. 1, case (2). Near the 2-3 interface the potential is repulsive in the more dense medium 2 and attractive in the more dilute medium 3. A new feature appears around the

center of the middle layer where a finite potential wall on the left and an attractive one towards the right interface combine to a potential well. Clearly, if an atom at rest is put in the well, it will remain there. When the thickness of the middle layer 2 is reduced, the well becomes more shallow and eventually disappears, as is visible in Figs. 5(b) and 5(c). For the parameters used in the figure, the potential well in the middle layer occurs when $d_2\omega_{10}/c \gg 1$ and is overwhelmed when $d_2\omega_{10}/c \sim 1$. The curves for the potential can help one to predict the movement of an atom located near or inside a membrane (layer 2). For example, let an atom be initially located in layer 3 (vacuum) of case (a). First, it will be attracted to the 2-3 interface. If it can be transported through the interface and gather enough momentum going down the slope, it can pass the finite potential wall and is then attracted to the 1-2 interface. After this interface, and maybe some oscillations, it will be suspended in the potential well near the surface.

We now turn to the symmetric configuration (right column of Fig. 5) where the middle layer 2 is sandwiched between two identical layers 1 and 3. The behavior of the potential on the right is just a mirror image of that on the left with the mirror plane being the one parallel to the surface and passing through the center of the middle layer. When the thickness of layer 2 is largest $d_2\omega_{10}/c=5$ [case (d)], we see in layer 2 a combination of two potential walls as found in Fig. 1, with a well in the middle. Thus, even as the middle layer is in general less dense than the two surrounding layers in both electric and magnetic aspects, there exists a possibility that an atom initially located in the potential well remains there. With decreasing thickness d_2, the bottom of the well rises and the two walls eventually merge into one [cases (e) and (f)]. Clearly, in cases (e) and (f), any atom initially situated in the middle layer will be transported to the neighboring layers. Numerical computation also shows that the magnitude of the position-independent term in $U_2(z_A)$—i.e., the last term in Eq. (20)—is negligible compared to the position-independent terms, due to the small exponential factor.

In Fig. 5, the uncorrected potentials are plotted by dashed lines. In the two outer layers, the effects of the local field almost remain the same as in the two-layer configuration, which can be explained by that the presence of a third layer is screened by the middle layer. For the middle layer, we have found that, typically, the local-field correction is most significant around the center of the layer, as is most manifest in case (f) where a correction $[(U_{2\text{corrected}} - U_{2\text{uncorrected}})/U_{2\text{uncorrected}}]$ of more than 80% is observed. A variation of the middle-layer thickness does not affect much the strength of the local-field correction near the surfaces. This can be understood as resulting from the fact that when an atom is located very close to a surface, it will tend to see only the nearest-neighboring layer.

If one wish to know the potentials right on the surfaces, one would have to evaluate the full potential $U_1+U_2(z_A)$ for atom-surface distances large enough such that the macroscopic theory applies and then use it as an input to the procedure proposed in the previous section. Since the position-independent part U_1 does not depend on the layer thicknesses, at each surface in a more-than-two-layer system, the results will be closely analogous to those of the two-layer case.

V. DISCUSSION AND SUMMARY

Our results might be of interest in biological applications such as the transfer of a small molecule through a membrane from one cell to another. Earlier theories have been developed to describe the vdW interaction between molecules or small particles and a solvent medium [8]. In particular, such particles were modeled by a small dielectric sphere of radius R_s and (macroscopic) permittivity ε_s. It was found that the nonretarded dispersion potential of such a sphere near the interface of two dielectric media (with the sphere being situated in a medium of permittivity ε_2, and ε_1 denoting the permittivity of the medium on the far side of the interface) is given by

$$U(z_s) = -\frac{\hbar}{16\pi^2\varepsilon_0 z_s^3}\int_0^\infty d\xi \frac{\alpha_s}{\varepsilon_2}\frac{\varepsilon_1-\varepsilon_2}{\varepsilon_1+\varepsilon_2}. \tag{54}$$

Here, z_s is the distance from the sphere to the surface and

$$\alpha_s(\omega) = 4\pi\varepsilon_0 R_s^3 \varepsilon_2(\omega)\frac{\varepsilon_s(\omega)-\varepsilon_2(\omega)}{\varepsilon_s(\omega)+2\varepsilon_2(\omega)} \tag{55}$$

is the excess or effective polarisability [32,33] of the dissolved particle in the medium. This potential already accounts for the fact that the (macroscopic) particle has a finite volume and can hence only move by displacing an equal volume of solvent from its path (with associated pressure forces being present); the excess polarizability and hence also the potential must vanish when a dissolved particle has the same properties as the solvent.

Equation (54) is the macroscopic counterpart of our microscopic equations (46)–(48), where the position-dependent part of our potential for purely dielectric solvent media reads

$$U_2(z_A) = -\frac{\hbar}{16\pi^2\varepsilon_0 z_A^3}\int_0^\infty d\xi \frac{\alpha}{\varepsilon_2}\left(\frac{3\varepsilon_2}{2\varepsilon_2+1}\right)^2\frac{\varepsilon_1-\varepsilon_2}{\varepsilon_1+\varepsilon_2}. \tag{56}$$

The results from a microscopic description of the particle as a system of bound point charges, leading to our Eq. (56), are thus formally very similar to those from a macroscopic model of the particle as a dielectric sphere, Eq. (54). The main difference is the fact that the microscopic polarizability (6) together with a local-field correction factor appears in Eq. (56), while the macroscopic excess polarizability (55) which effectively accounts for pressure forces enters Eq. (54). Depending on the size of the immersed particle, one of the two models may provide a more realistic description: For very small particles such as atoms or small molecules whose size is comparable to the free interspaces between the atoms forming the solvent medium, local-field effects are important, while (macroscopic) pressure forces cannot even be defined, so that the microscopic result (56) should be used. For larger molecules whose volume covers a region that would otherwise be occupied by a large number of solvent atoms, local-field effects can be neglected while pressure forces become relevant, so Eq. (54) should be given preference. As an additional difference, note that our microscopic calculation has also given layer-dependent constant contributions to the potential, which are absent in Eq. (54).

Similar considerations apply in the retarded limit, where the macroscopic potential of the small sphere was found to be [8]

$$U(z_s) = -\frac{23\hbar c}{320\pi^2\varepsilon_0 z_s^4}\frac{\alpha_s(0)}{\varepsilon_2^{3/2}(0)}\frac{\varepsilon_1(0)-\varepsilon_2(0)}{\varepsilon_1(0)+\varepsilon_2(0)}, \tag{57}$$

whereas our microscopic result as given by Eqs. (28) and (29) reads

$$U_2(z_A) = \frac{3\hbar c}{64\pi^2\varepsilon_0 z_A^4}\frac{\alpha(0)}{\varepsilon_1^{3/2}(0)}\left[\frac{3\varepsilon_2(0)}{2\varepsilon_2(0)+1}\right]^2 \times \int_1^\infty dy\left[\left(\frac{1}{y^4}-\frac{2}{y^2}\right)\frac{ay-\sqrt{y^2-1+a}}{ay+\sqrt{y^2-1+a}} + \frac{1}{y^4}\frac{y-\sqrt{y^2-1+a}}{y+\sqrt{y^2-1+a}}\right] \tag{58}$$

$[a=\varepsilon_1(0)/\varepsilon_2(0)]$. In addition to the observations made for the nonretarded limit, the interface-dependent proportionality constants [i.e., the last factors in Eqs. (57) and (58)] are now also different in general; note that they do agree in the limit of small dielectric contrast between the media, $\chi(0)=\varepsilon_1(0)-\varepsilon_2(0)\ll\varepsilon_2(0)$.

To conclude, we have the local-field-corrected vdW potential of a ground-state atom embedded in a planar magnetodielectric multilayer system by analytical and numerical means. The theory allows us to extend earlier studies of the same system in two important aspects: first, one can allow for the atom to be embedded in a medium, thus making the theory applicable to a larger range of realistic situations; second, the effects of the local-field correction are elucidated.

The formulas for the interaction potential have been derived for an arbitrary number of layers where the cases of two- and three-layer systems have been studied in detail. We have shown that the potential can be decomposed into two parts: a layer-dependent constant part which depends on the real-cavity radius—i.e., the density of the medium the atom is placed in—and a position-dependent part that contains the local-field correction as a factor in the integral over frequency. For the latter, we have presented retarded and nonretarded limits and the considered case of neighboring media of similar properties. Distance laws have been reestablished with effects of the local field included where the local-field correction has been found to be as high as 80% in certain cases. Further, numerical calculations show that an interplay between electric and magnetic properties of the neighboring media may lead to the appearance of potential wells or walls near the surface. These structures are potentially helpful as a trapping mechanism. Although these structures are much less intense in magnitude than those occurring for an excited atom [28,29], they are more permanent because an atom in the ground state has an infinitely long lifetime.

The constant part of the potential, which originates from local-field effects, does not contribute to the vdW forces, but it can facilitate our understanding of the movement of an atom near an interface and is instrumental in our proposed estimate of the on-surface value of the potential: After calculating the total potential in both sides of an interface up to distances equal to the radius of the (real) cavity, beyond which a macroscopic model no longer applies, the average of the two potential values taken at these distances can be regarded as the potential at the interface. Our procedure improves previous similar estimates by including local-field effects and consistently removing self-interactions.

In the case of the three-layer system, emphasis was given to the influence of the thickness of the middle layer. While new features may arise for a very thin middle layer, the behavior of the potential is simply that at the interfaces combined if the middle layer is thick enough.

Our results, which have been obtained on the basis of an exact, microscopic model of the atom-field coupling, are complementary to previous more macroscopic dispersion potentials of particles modeled as small spheres. The model of preference depends on the size of the particle in the specific situations considered. In the future, efforts should be taken to find a dispersion potential which holds for all possible ranges of particle sizes and includes both the microscopic and macroscopic potentials as limiting cases. Our considerations may easily be extended to other geometries, such as spherically or cylindrically layered host media.

ACKNOWLEDGMENTS

The work was supported by Deutsche Forschungsgemeinschaft. S.Y.B. and H.T.D. are grateful to the Alexander von Humboldt Stiftung for support.

[1] S. Y. Buhmann and D.-G. Welsch, Prog. Quantum Electron. **31**, 51 (2007).
[2] H. B. G. Casimir and D. Polder, Phys. Rev. **73**, 360 (1948).
[3] T. F. Tadros, Adv. Colloid Interface Sci. **46**, 1 (1993).
[4] J. Gregory, Water Sci. Technol. **27**, 1 (1993).
[5] D. N. Thomas, S. J. Judd, and N. Fawcett, Water Res. **33**, 1579 (1999).
[6] G. V. Lubarsky, S. A. Mitchell, M. R. Davidson, and R. Bradley, Colloids Surf., A **279**, 188 (2006).
[7] S. Nir, Prog. Surf. Sci. **8**, 1 (1976).
[8] J. N. Israelachvili, Q. Rev. Biophys. **6**, 341 (1974).
[9] M. S. Tomaš, Phys. Rev. A **75**, 012109 (2007).
[10] A. Sambale, S. Y. Buhmann, D.-G. Welsch, and M.-S. Tomaš, Phys. Rev. A **75**, 042109 (2007).
[11] L. Onsager, J. Am. Chem. Soc. **58**, 1486 (1936).
[12] H. J. Lezec, J. A. Dionne, and H. A. Atwater, Science **316**, 430 (2007).
[13] M. S. Tomaš, J. Phys. A **41**, 164020 (2007).
[14] G. G. Kleiman and U. Landman, Phys. Rev. B **8**, 5484 (1973).
[15] E. Zaremba and W. Kohn, Phys. Rev. B **15**, 1769 (1977).
[16] P. Nordlander and J. Harris, J. Phys. C **17**, 1141 (1984).
[17] C. Holmberg and P. Apell, Phys. Rev. B **30**, 5721 (1984).

[18] S. Das Sarma and S.-M. Paik, Chem. Phys. Lett. **126**, 526 (1986).
[19] C. Holmberg, P. Apell, and J. Giraldo, Phys. Scr. **33**, 173 (1986).
[20] G. Mukhopadhyay, Phys. Scr. **36**, 676 (1987).
[21] E. M. Lifshitz, Sov. Phys. JETP **29**, 94 (1955).
[22] S. Y. Buhmann, D.-G. Welsch, and T. Kampf, Phys. Rev. A **72**, 032112 (2005).
[23] E. Zaremba and W. Kohn, Phys. Rev. B **13**, 2270 (1976).
[24] G. Mukhopadhyay and J. Mahanty, Solid State Commun. **16**, 597 (1975).
[25] C. Holmberg and P. Apell, Solid State Commun. **49**, 513 (1984).
[26] V. M. Fain and Y. I. Khanin, *Quantum Electronics* (MIT Press, Cambridge, MA, 1969).
[27] S. Spagnolo, D. A. R. Dalvit, and P. W. Milonni, Phys. Rev. A **75**, 052117 (2007).
[28] A. Sambale, D.-G. Welsch, Ho Trung Dung, and S. Y. Buhmann, Phys. Rev. A **78**, 053828 (2008).
[29] A. Sambale, D.-G. Welsch, Ho Trung Dung, and S. Y. Buhmann, Phys. Scr. (to be published), e-print arXiv:0809.3086.
[30] D. Langbein, *Theory of Van der Waals Attraction* (Springer, Berlin, 1974).
[31] J. Mahanty and B. W. Ninham, *Dispersion Forces* (Academic Press, London, 1976).
[32] A. D. McLachlan, Discuss. Faraday Soc. **40**, 239 (1965).
[33] L. D. Landau and E. M. Lifshitz, *Electrodynamics of Continuous Media*, 2nd ed. (Pergamon Press, Oxford 1984), Vol. 8.